

The cosmic-ray electron flux measured by the PAMELA experiment between 1 and 625 GeV

O. Adriani,^{1,2} G. C. Barbarino,^{3,4} G. A. Bazilevskaya,⁵ R. Bellotti,^{6,7} M. Boezio,⁸ E. A. Bogomolov,⁹ M. Bongi,² V. Bonvicini,⁸ S. Borisov,^{10,11,12} S. Bottai,² A. Bruno,^{6,7} F. Cafagna,⁷ D. Campana,⁴ R. Carbone,^{4,11} P. Carlson,¹³ M. Casolino,¹⁰ G. Castellini,¹⁴ L. Consiglio,⁴ M. P. De Pascale,^{10,11} C. De Santis,¹⁰ N. De Simone,^{10,11} V. Di Felice,¹⁰ A. M. Galper,¹² W. Gillard,¹³ L. Grishantseva,¹² G. Jerse,^{8,15} A. V. Karelin,¹² S. V. Koldashov,¹² S. Y. Krutkov,⁹ A. N. Kvashnin,⁵ A. Leonov,¹² V. Malakhov,¹² V. Malvezzi,¹⁰ L. Marcelli,¹⁰ A. G. Mayorov,¹² W. Menn,¹⁶ V. V. Mikhailov,¹² E. Mocchiutti,⁸ A. Monaco,^{6,7} N. Mori,^{1,2} N. Nikonov,^{9,10,11} G. Osteria,⁴ F. Palma,^{10,11} P. Papini,² M. Pearce,¹³ P. Picozza,^{10,11} C. Pizzolotto,⁸ M. Ricci,¹⁷ S. B. Ricciarini,² L. Rossetto,¹³ R. Sarkar,⁸ M. Simon,¹⁶ R. Sparvoli,^{10,11} P. Spillantini,^{1,2} S. J. Stochaj,¹⁸ J. C. Stockton,¹⁸ Y. I. Stozhkov,⁵ A. Vacchi,⁸ E. Vannuccini,² G. Vasilyev,⁹ S. A. Voronov,¹² J. Wu,^{13,*} Y. T. Yurkin,¹² G. Zampa,⁸ N. Zampa,⁸ and V. G. Zverev¹²

¹*University of Florence, Department of Physics,
I-50019 Sesto Fiorentino, Florence, Italy*

²*INFN, Sezione di Florence, I-50019 Sesto Fiorentino, Florence, Italy*

³*University of Naples “Federico II”,
Department of Physics, I-80126 Naples, Italy*

⁴*INFN, Sezione di Naples, I-80126 Naples, Italy*

⁵*Lebedev Physical Institute, RU-119991 Moscow, Russia*

⁶*University of Bari, Department of Physics, I-70126 Bari, Italy*

⁷*INFN, Sezione di Bari, I-70126 Bari, Italy*

⁸*INFN, Sezione di Trieste, I-34149 Trieste, Italy*

⁹*Ioffe Physical Technical Institute, RU-194021 St. Petersburg, Russia*

¹⁰*INFN, Sezione di Rome “Tor Vergata”, I-00133 Rome, Italy*

¹¹*University of Rome “Tor Vergata”,*

Department of Physics, I-00133 Rome, Italy

¹²*National Research Nuclear University “MEPHI”, RU-115409 Moscow, Russia*

¹³*KTH, Department of Physics, and the Oskar Klein Centre for Cosmoparticle Physics,*

AlbaNova University Centre, SE-10691 Stockholm, Sweden

¹⁴ *IFAC, I-50019 Sesto Fiorentino, Florence, Italy*

¹⁵ *University of Trieste, Department of Physics, I-34147 Trieste, Italy*

¹⁶ *Universität Siegen, Department of Physics, D-57068 Siegen, Germany*

¹⁷ *INFN, Laboratori Nazionali di Frascati,*

Via Enrico Fermi 40, I-00044 Frascati, Italy

¹⁸ *New Mexico State University, Las Cruces, NM 88003, USA*

(Dated: October 24, 2018)

Abstract

Precision measurements of the electron component in the cosmic radiation provide important information about the origin and propagation of cosmic rays in the Galaxy. Here we present new results regarding negatively charged electrons between 1 and 625 GeV performed by the satellite-borne experiment PAMELA. This is the first time that cosmic-ray e^- have been identified above 50 GeV. The electron spectrum can be described with a single power law energy dependence with spectral index -3.18 ± 0.05 above the energy region influenced by the solar wind (> 30 GeV). No significant spectral features are observed and the data can be interpreted in terms of conventional diffusive propagation models. However, the data are also consistent with models including new cosmic-ray sources that could explain the rise in the positron fraction.

PACS numbers: 98.70.Sa, 96.50.sb, 95.35.+d

Cosmic-ray electrons are a small but important component of the cosmic radiation. They provide information regarding the origin and propagation of cosmic rays in the Galaxy that is not accessible from the study of the cosmic-ray nuclear components due to their differing energy-loss processes. Cosmic-ray electrons and positrons are produced as secondaries by the interactions between cosmic-ray nuclei and the interstellar matter. However, since the observed positron fraction ($\phi(e^+) / (\phi(e^+) + \phi(e^-))$), where ϕ is the flux, is of the order of ten percent and less above a few GeV [1–3], a majority of electrons must be of primary origin.

Due to their low mass and the intergalactic magnetic field, cosmic-ray electrons undergo severe energy losses during their propagation in the Galaxy. Therefore, it can be expected that a significant fraction of high energy (> 10 GeV) electrons and positrons are produced in the solar neighborhood (~ 1 kpc) [4] with the majority of the primary electron component probably originating from a small number of sources, which may induce features in the spectral shape of the electron energy spectrum [5, 6]. Spectral features may also arise from the contribution of more exotic sources such as dark matter particles, e.g. [7], or other astrophysical objects such as pulsars, e.g. [8]. Both were invoked to explain the positron fraction measured by PAMELA [3] and are expected to contribute to the cosmic radiation with roughly equal numbers of electrons and positrons.

Measuring the energy spectrum of cosmic-ray electrons involves the difficult identification of this rare component and determination of detector efficiencies and particle energies. Therefore, it is not a surprise that results, gathered mostly by balloon-borne experiments in the past decades, differ beyond quoted errors. Another point that has to be highlighted is that there are no measurements of the high energy (above ~ 50 GeV) negatively-charged electron flux.

The results presented here are based on the data-set collected by the PAMELA satellite-borne experiment between July 2006 and January 2010. From over 2×10^9 triggered events, accumulated during a total acquisition time of approximately 1200 days, 377,614 electrons were selected in the energy interval 1 - 625 GeV, the largest energy range covered in any cosmic ray e^- experiment hitherto. Further details on the PAMELA apparatus, orbit and data acquisition can be found in [9–11].

A sample of negatively-charged particles was selected using the time-of-flight and spectrometer data. This consisted mostly of electrons with a few percent contamination of

cosmic-ray antiprotons. At higher rigidities “spillover” protons, reconstructed with an incorrect sign of curvature either due to the finite spectrometer resolution or scattering in the spectrometer planes, represented the largest source of contamination estimated to increase from a few percent at ~ 100 GV/c to about ten times the electron signal around 500 GV/c. All these contamination components were reduced to a negligible amount by requiring an electromagnetic-like interaction pattern in the 16 radiation length deep silicon-tungsten calorimeter [10, 12]. Electrons were selected up to ~ 600 GV/c. Above this rigidity the sign-of-curvature of tracks could not be reliably resolved due to statistical and systematic uncertainties.

The most important contributions to the discrepancies between the various electron measurements are instrumental effects such as selection efficiencies and energy determination. To reduce the systematic uncertainties the selection efficiencies were derived from flight data, cross-checking the results with those obtained using simulations of the apparatus based both on the GEANT3 [13] and GEANT4 [14] packages. The validity of the simulations was confirmed by comparisons with test-beam and flight data. The simulations were also used in PAMELA results concerning antiprotons, protons and helium nuclei [11, 15]. The total systematic uncertainty on the flux was found to increase from about 4% at 1 GV/c to about 7% at 600 GV/c. This uncertainty was obtained quadratically summing the various systematic errors considered: acceptance, efficiency estimation and spectrum unfolding. The energy-binned electron fluxes are given in Table I. These results were obtained using the rigidity measured by the magnetic spectrometer and unfolding the resulting energy spectrum to the top of the payload using a Bayesian approach, as described in [17]. This unfolding was particularly important for electrons (and positrons) due to their non-negligible energy losses, primarily due to bremsstrahlung while traversing the pressurised container and parts of the apparatus prior to the tracking system (equivalent to about 0.1 radiation lengths).

Since the PAMELA calorimeter was also designed to precisely sample the total energy deposited by electromagnetic showers [18], this information was used to derive the energy of the impinging electron. Containment requirements (at least half Moliere radii from the silicon detector borders for each calorimeter layer) were applied to the projected track in the calorimeter. This resulted in a good Gaussian energy resolution, varying from $\simeq 8\%$ at 10 GeV to $\simeq 3\%$ above 100 GeV, but also in a decrease in statistics of $\simeq 50\%$. Hence, it was possible to obtain an estimation of the energy of cosmic-ray electrons that was systemati-

TABLE I: Summary of electron results. The first and second errors represent the statistical and systematic uncertainties, respectively. The mean kinetic energy has been obtained following the procedure described in [16].

Rigidity at the spectrometer GV/c	Mean Kinetic Energy at top of payload GeV	Observed number of events	Flux at top of payload (particles/(m ² sr s GeV))
1.04 - 1.19	1.11	27930	31.2 ± 0.2 ± 1.3
1.19 - 1.37	1.28	30361	26.7 ± 0.2 ± 1.1
1.37 - 1.57	1.47	32973	23.0 ± 0.1 ± 1.0
1.57 - 1.80	1.68	33787	18.8 ± 0.1 ± 0.8
1.80 - 2.07	1.93	33613	15.03 ± 0.08 ± 0.6
2.07 - 2.38	2.22	32854	11.94 ± 0.07 ± 0.5
2.38 - 2.73	2.55	30118	8.97 ± 0.05 ± 0.4
2.73 - 3.13	2.92	27234	6.67 ± 0.04 ± 0.3
3.13 - 3.60	3.36	23607	4.76 ± 0.03 ± 0.2
3.60 - 4.13	3.85	20440	3.40 ± 0.02 ± 0.1
4.13 - 4.74	4.42	16817	2.30 ± 0.02 ± 0.1
4.7 - 5.4	5.1	13812	1.56 ± 0.01 ± 0.07
5.4 - 6.3	5.8	11428	1.06 ± 0.01 ± 0.05
6.3 - 7.2	6.7	9410	(7.2 ± 0.07 ± 0.3) × 10 ⁻¹
7.2 - 8.2	7.7	7374	(4.7 ± 0.05 ± 0.2) × 10 ⁻¹
8.2 - 9.5	8.8	5851	(3.1 ± 0.04 ± 0.1) × 10 ⁻¹
9.5 - 10.9	10.1	4441	(1.91 ± 0.03 ± 0.08) × 10 ⁻¹
10.9 - 12.5	11.6	3583	(1.26 ± 0.02 ± 0.05) × 10 ⁻¹
12.5 - 14.3	13.4	2767	(7.9 ± 0.2 ± 0.3) × 10 ⁻²
14.3 - 16.4	15.3	2266	(5.2 ± 0.1 ± 0.2) × 10 ⁻²
16.4 - 18.9	17.6	1798	(3.26 ± 0.08 ± 0.1) × 10 ⁻²
18.9 - 21.7	20.2	1392	(2.08 ± 0.06 ± 0.09) × 10 ⁻²
21.7 - 24.9	23.2	972	(1.26 ± 0.04 ± 0.05) × 10 ⁻²
24.9 - 28.6	26.6	778	(8.9 ± 0.3 ± 0.4) × 10 ⁻³
28.6 - 32.8	30.6	518	(5.2 ± 0.2 ± 0.2) × 10 ⁻³
32.8 - 37.7	35.1	422	(3.7 ± 0.2 ± 0.2) × 10 ⁻³
37.7 - 43.3	40.3	276	(2.2 ± 0.1 ± 0.09) × 10 ⁻³
43.3 - 49.7	46.3	211	(1.4 ± 0.1 ± 0.06) × 10 ⁻³
49.7 - 57.0	53.2	172	(1.04 ± 0.08 ± 0.04) × 10 ⁻³
57.0 - 65.5	61.0	104	(5.5 ± 0.5 ± 0.2) × 10 ⁻⁴
65.5 - 75.2	70.1	87	(4.1 ± 0.4 ± 0.2) × 10 ⁻⁴
75.2 - 86.3	80.5	52	(2.1 ± 0.3 ± 0.09) × 10 ⁻⁴
86.3 - 99.1	92.4	42	(1.5 ± 0.2 ± 0.07) × 10 ⁻⁴
99.1 - 119.1	108.5	41	(10. ± 2. ± 0.4) × 10 ⁻⁵
119.1 - 143.2	130.4	33	(7. ± 1. ± 0.3) × 10 ⁻⁵
143.2 - 188.8	163.8	25	(2.7 ± 0.5 ± 0.1) × 10 ⁻⁵
188.8 - 260.7	220.7	14	(9.6 ^{+3.0} _{-2.5} ± 0.5) × 10 ⁻⁶
260.7 - 394.5	317.9	7	(2.8 ^{+1.3} _{-1.1} ± 0.1) × 10 ⁻⁶
394.5 - 625.3	491.4	3	(9 ⁺⁷ ₋₆ ± 1) × 10 ⁻⁷

cally independent of the rigidity measurement, The bremsstrahlung photons, produced by electrons while crossing the top part of the payload, converted into electromagnetic showers in the calorimeter, thus allowing the total energy of the incoming electron to be estimated. Therefore, the calorimetry measurement provided a cross-check of the energy spectrum derived from the tracking system information.

Figure 1 shows the electron energy spectra obtained using the calorimeter and the tracking information. The sign of the curvature in the magnetic spectrometer was used to select negative particles also for the calorimeter case, thus making a consistent comparison possible. The two sets of measurements are in good agreement considering the uncertainty of the

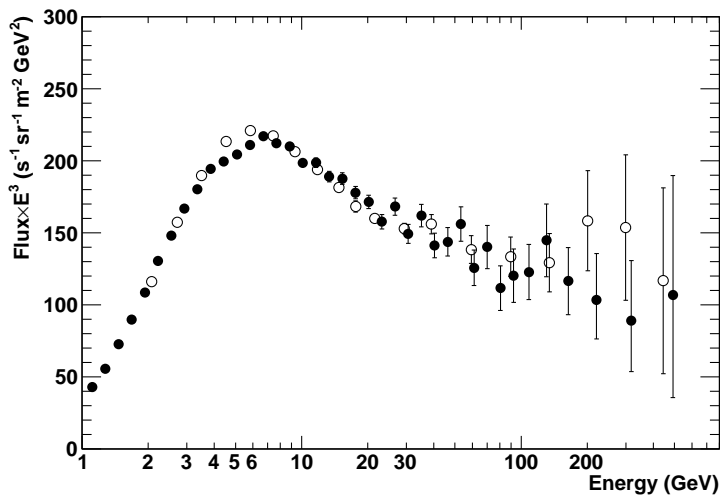


FIG. 1: The negatively-charged electron spectrum measured by PAMELA with two independent approaches: energy derived from the rigidity (full circles); energy derived from the calorimeter information (open circles). The error bars are statistical only.

reconstruction and unfolding procedures. The results discussed in this work are based on the magnetic spectrometer rigidity that provided a larger statistical sample and a better energy resolution in the most statistically significant energy region.

Figure 2 shows the electron energy spectrum measured by PAMELA along with other recent experimental data [19–27]. The data from [23–27] and the highest data point from HEAT [20] refer to the sum of electron and positron fluxes. Considering statistical and systematic uncertainties, no significant disagreements are found between PAMELA and the recent ATIC [25] and Fermi [27] data, even considering an additional positron component in

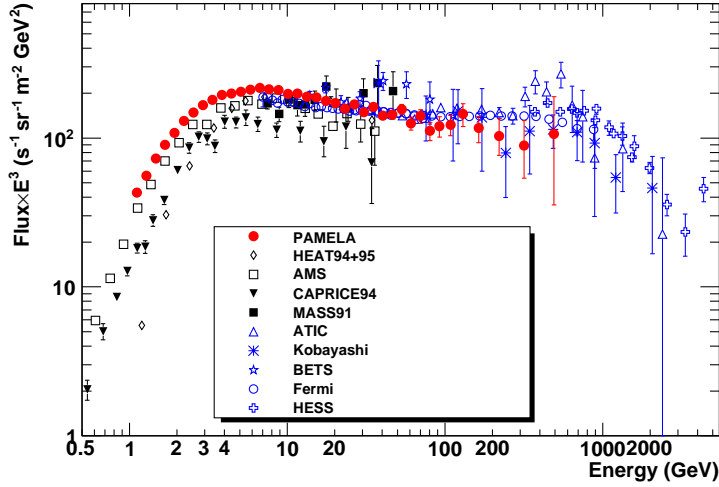


FIG. 2: The electron energy spectrum obtained in this work compared with modern measurements: CAPRICE94 [19], HEAT [20], AMS [21], MASS91 [22], Kobayashi [23], BETS [24], ATIC [25], HESS [26], Fermi [27]. Note that the data points from [23–27], indicated with blue symbols, and the highest data point from HEAT [20] are for the electron and positron sum.

these measurements of order a few percent (see [28]). However, the PAMELA e^- spectrum appears softer than the $(e^- + e^+)$ spectra presented by ATIC and Fermi. This difference is within the systematic uncertainties between the various measurements, but it is also consistent with a growing positron component with energy. An analysis of the PAMELA positron energy spectrum (up to ~ 300 GeV) will be presented in a future publication. The differences with previous magnetic-spectrometer measurements [19–22] are larger and probably due to uncertainties in the energy and efficiencies determination of the various experiments. Below 10 GeV, discrepancies can be partially explained by the effect of solar modulation for the various data taking periods.

Figure 3 top shows the PAMELA e^- spectrum compared with a theoretical calculation (solid line) based on the GALPROP code [29] and with a single power-law fit (long-dashed line) to the data above 30 GeV (above the influence of solar modulation). The single power-law fit represents well the data ($\chi^2/\text{ndf} = 8.7/13$) with a resulting spectral index of -3.18 ± 0.05 . This is incompatible (about 6 standard deviation discrepancy even considering systematic errors) with the soft e^- spectrum [4] required to explain the PAMELA positron fraction measurement within a standard model of cosmic-ray propagation. The

GALPROP calculation was performed using a spatial Kolmogorov diffusion with spectral index $\delta = 0.34$ and diffusive reacceleration characterized by an Alfvén speed $v_A = 36$ km/s and halo height of 4 kpc (parameters from [30]). The injection e^- spectrum (spectral index: -2.66) was obtained from a best fit of the propagated spectrum to PAMELA results, which was normalized to the data at ~ 70 GeV and calculated for solar minimum, using the force field approximation [31] ($\Phi = 600$ MV). For secondary e^- production during propagation we used primary proton and helium spectra that reproduced PAMELA measurements [15]. This GALPROP calculation reproduces fairly well the results above 10 GeV ($\chi^2/\text{ndf} = 35/26$), however differences between the measured and predicted spectral shapes can be noticed. This may indicate that changes in the propagation model or additional

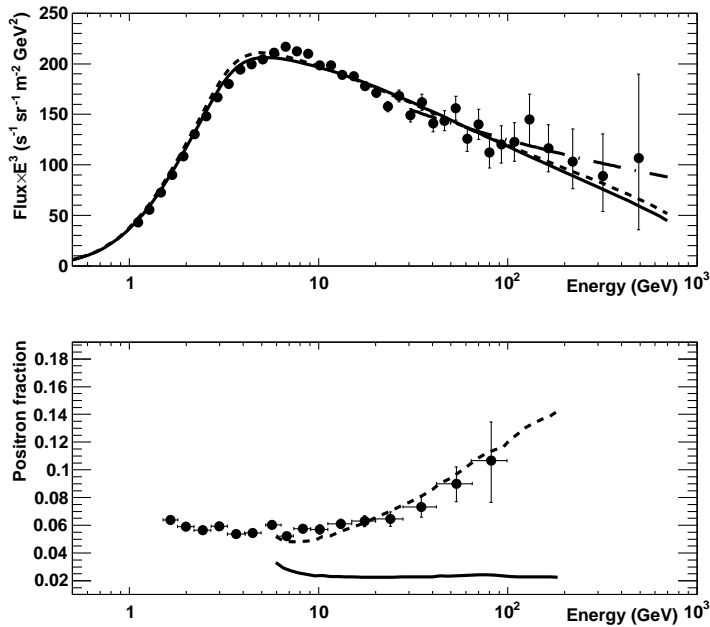


FIG. 3: Top: the e^- spectrum obtained in this work compared with theoretical calculations. The solid line shows the standard GALPROP calculation [29] for a diffusion reacceleration model; the long-dashed line is a single power-law fit to the data above 30 GeV; the short-dashed line is a GALPROP calculation including a component from additional cosmic-ray electron sources. Bottom: the PAMELA positron fraction [28] compared with the previous GALPROP calculations with no (solid line) and with additional e^- and e^+ components (short-dashed line). The error bars are statistical only and these were the only errors considered by the fitting procedures.

sources of cosmic-ray electrons are needed. The GALPROP calculation is commonly used

assuming a continuous distribution of sources in the Galaxy. However, due to the significant energy losses this does not seem plausible for primary high energy electrons [33], since this assumption should only hold for a relatively close neighborhood. Furthermore, as pointed out in [32], SNRs are concentrated in the spiral arms of the Galaxy, therefore one should consider an inhomogeneous source distribution.

One important point concerning sources of primary e^+ invoked to explain the positron fraction measurement [3], is that they should contribute to both the e^+ and e^- components in about equal amount. It is therefore reasonable to investigate if the PAMELA e^- data can accommodate an additional component consistent with the positron fraction [28]. Hence, we repeated the previous GALPROP calculation including an e^- component resulting from new sources for which the only assumption was that they injected e^- and e^+ in the interstellar medium with a power law energy spectrum. The best fit to the data indicated that a model (short-dashed line in Figure 3 top) with three components: two primary electron components with different injection spectra (2.69 ± 0.04 and 2.1 ± 0.4) and secondary electrons, provided a better agreement to PAMELA data ($\chi^2/\text{ndf} = 30.9/27$) than the standard, two component GALPROP calculation (solid line). Furthermore, assuming that the new primary component, which dominated the high energy region with a harder spectrum, identically contributed to the positron component we were able to reproduce PAMELA positron fraction [28] above 5 GeV. Figure 3 bottom shows this positron fraction compared to the GALPROP predictions with no (solid line) and with additional e^- and e^+ components (short-dashed line).

We have measured the e^- energy spectrum over the broadest energy range ever achieved and with no atmospheric overburden. Our results are not inconsistent with the standard model of cosmic ray acceleration and propagation in the Galaxy. However, there is some tension between the data and the prediction that points to needed refinements of the propagation models and might require additional sources of cosmic rays.

We acknowledge support from The Italian Space Agency (ASI), Deutsches Zentrum für Luft- und Raumfahrt (DLR), The Swedish National Space Board, The Swedish Research Council, The Russian Space Agency (Roscosmos) and The Russian Foundation for Basic Research. R. S. wishes to thank the TRIL program of the International Center of Theoretical Physics, Trieste, Italy that partly sponsored his activity.

* On leave from School of Mathematics and Physics, China University of Geosciences, CN-430074
Wuhan, China

- [1] J. A. D. Shong, R. H. Hildebrand, and P. Meyer, *Phys. Rev. Lett.* **12**, 3 (1964).
- [2] J. L. Fanelow, R. C. Hartman, R. H. Hildebrand, and P. Meyer, *Astrophys. J.* **158**, 771 (1969).
- [3] O. Adriani et al., *Nature* **458**, 607 (2009).
- [4] T. Delahaye, F. Donato, N. Fornengo, J. Lavalle, R. Lineros, P. Salati, and R. Taillet, *Astron. Astrophys.* **501**, 821 (2009).
- [5] J. Nishimura et al., *Astrophys. J.* **238**, 394 (1980).
- [6] T. Delahaye, J. Lavalle, R. Lineros, F. Donato, and N. Fornengo, *Astron. Astrophys.* **524**, A51 (2010).
- [7] M. Cirelli, M. Kadastik, M. Raidal, and A. Strumia, *Nucl. Phys. B* **813**, 1 (2008).
- [8] A. M. Atoyan, F. A. Aharonian, and H. J. Volk, *Phys. Rev. D* **52**, 3265 (1995).
- [9] P. Picozza et al., *Astropart. Phys.* **27**, 296 (2007).
- [10] M. Boezio et al., *New J. Phys.* **11**, 105023 (2009).
- [11] O. Adriani et al., *Phys. Rev. Lett.* **105**, 121101 (2010).
- [12] M. Boezio et al., *Astropart. Phys.* **26**, 111 (2006).
- [13] R. Brun et al., Detector description and simulation tool, CERN program library (1994), version 3.21.
- [14] S. Agostinelli et al., *Nucl. Instrum. Meth. A* **506**, 250 (2003).
- [15] O. Adriani et al., accepted for publication in *Science*.
- [16] G. D. Lafferty and T. T. Wyatt, *Nucl. Instrum. Meth. A* **355**, 541 (1995).
- [17] G. D'Agostini, *Nucl. Instrum. Meth. A* **362**, 487 (1995).
- [18] M. Boezio, V. Bonvicini, E. Mocchiutti, P. Schiavon, G. Scian, A. Vacchi, G. Zampa, and N. Zampa, *Nucl. Instrum. Meth. A* **487**, 407 (2002).
- [19] M. Boezio et al., *Astrophys. J.* **532**, 653 (2000).
- [20] M. A. DuVernois et al., *Astrophys. J.* **559**, 296 (2001).
- [21] J. Alcaraz et al., *Phys. Lett. B* **484**, 10 (2000).
- [22] C. Grimani et al., *Astron. Astrophys.* **392**, 287 (2002).
- [23] T. Kobayashi, J. Nishimura, Y. Komori, T. Shirai, N. Tateyama, T. Taira, K. Yoshida, and

- T. Yuda, in Proc. 26th Int. Cosmic Ray Conf. (Salt Lake City) (1999), vol. 3, p. 61.
- [24] S. Torii et al., *Astrophys. J.* **559**, 973 (2001).
 - [25] J. Chang et al., *Nature* **456**, 362 (2008).
 - [26] F. Aharonian et al., *Phys. Rev. Lett.* **101**, 261104 (2008).
 - [27] M. Ackermann et al., *Phys. Rev. D* **82**, 092004 (2010).
 - [28] O. Adriani et al., *Astropart. Phys.* **34**, 1 (2010).
 - [29] A. W. Strong and I. V. Moskalenko, *Astrophys. J.* **509**, 212 (1998).
 - [30] V. S. Ptuskin et al., *Astrophys. J.* **642**, 902 (2006).
 - [31] L. J. Gleeson and W. I. Axford, *Astrophys. J.* **154**, 1011 (1968).
 - [32] N. J. Shaviv, E. Nakar, and T. Piran, *Phys. Rev. Lett.* **103**, 111302 (2009).
 - [33] On the contrary this is valid for secondary e^- and e^+ since the cosmic-ray protons and nuclei interact with the ambient gas fairly uniformly in the interstellar medium.